PTEP

Prog. Theor. Exp. Phys. **2022** 023B05(12 pages)
DOI: 10.1093/ptep/ptac001

Role of the axial $U(1)$ anomaly in the chiral susceptibility of QCD at high temperature

S. Aoki[1], Y. Aoki[2], H. Fukaya[3,⋆], S. Hashimoto[4,5], C. Rohrhofer[3], K. Suzuki[6], JLQCD Collaboration

[1] *Center for Gravitational Physics, Yukawa Institute for Theoretical Physics, Kyoto University, Kyoto 606-8502, Japan*
[2] *RIKEN Center for Computational Science, 7-1-26 Minatojima-minami-machi, Chuo-ku, Kobe, Hyogo 650-0047, Japan*
[3] *Department of Physics, Osaka University, Toyonaka 560-0043, Japan*
[4] *High Energy Accelerator Research Organization (KEK), Tsukuba 305-0801, Japan*
[5] *School of High Energy Accelerator Science, The Graduate University for Advanced Studies (Sokendai), Tsukuba 305-0801, Japan*
[6] *Advanced Science Research Center, Japan Atomic Energy Agency (JAEA), Tokai 319-1195, Japan*
⋆E-mail: hfukaya@het.phys.sci.osaka-u.ac.jp

Received September 28, 2021; Revised December 23, 2021; Accepted January 12, 2022; Published January 14, 2022

The chiral susceptibility, or the first derivative of the chiral condensate with respect to the quark mass, is often used as a probe for the QCD phase transition since the chiral condensate is an order parameter of $SU(2)_L \times SU(2)_R$ symmetry breaking. However, the chiral condensate also breaks the axial $U(1)$ symmetry, which is usually not studied as it is already broken by the anomaly and apparently has little impact on the transition. We investigate the susceptibilities in the scalar and pseudoscalar channels in order to quantify how much the axial $U(1)$ breaking contributes to the chiral phase transition. Employing a chirally symmetric lattice Dirac operator and its eigenmode decomposition, we separate the axial $U(1)$ breaking effects from others. Our result in two-flavor QCD indicates that both of the connected and disconnected chiral susceptibilities are dominated by axial $U(1)$ breaking at temperatures $T \gtrsim 190$ MeV after the quadratically divergent constant is subtracted.

Subject Index B01, B02, B64, D31

1. Introduction

The properties of phase transition are largely governed by symmetries that are broken/restored at the transition. In quantum chromodynamics (QCD) with two degenerate dynamical quarks (up and down), the relevant symmetry is that of flavor rotation of left- and right-handed quark fields, i.e., $SU(2)_L \times SU(2)_R$ chiral symmetry, which is spontaneously broken at low temperatures but is believed to be recovered at some high temperature experienced by our universe at its early stage. The chiral condensate $\Sigma(m) = -\sum_x \langle S^0(x)\rangle/V$, defined with a flavor singlet scalar quark bilinear operator $S^0(x)$ and the four-volume V, as well as its derivative $\chi(m) = \frac{\partial}{\partial m}\Sigma(m)$, known as the chiral susceptibility, are often used to probe the so-called chiral phase transition [1–9].

The condensate also breaks the flavor-singlet axial symmetry $U(1)_A$ but its relevance is not immediately clear, since it is broken by the quantum anomaly, which exists at any energy scale. The $U(1)_A$ anomaly may still affect the low-energy dynamics as it is related to the topology of

Funded by SCOAP[3]

the gluon field and the zero eigenstates of the Dirac operator through the index theorem. In fact, the founders of QCD (see, e.g., Ref. [10]) strongly suggested that the $SU(2)_L \times SU(2)_R$ breaking is triggered by the topologically nontrivial configuration of gluons and a quantitative estimate was even made in Ref. [11]. However, this view of the $U(1)_A$ anomaly as the origin of the $SU(2)_L \times SU(2)_R$ breaking is not widely appreciated today since early lattice simulations reported survival of the axial $U(1)$ anomaly near the critical temperature; thus, the $U(1)_A$ anomaly apparently has little impact on the transition.

In this work, we revisit this issue, using lattice QCD with exactly chiral and flavor symmetric quarks. The index theorem is satisfied on the lattice to good precision so that the relation between topological gauge excitation and the fermion near-zero mode remains intact. By an eigenmode decomposition of the Dirac operator and quark propagators [12–15], we can unambiguously separate the $U(1)_A$ breaking effect from others in the chiral susceptibility $\chi(m) = \sum_x \langle S^0(x) S^0(0)\rangle - V\langle S^0(0)\rangle^2$. With the exact chiral symmetry, we can avoid severe lattice artifacts that can induce large overestimates of the $U(1)_A$ breaking as demonstrated in Refs. [13,14].

We find that $\chi(m)$ in the high-temperature phase mostly probes the presence/absence of the $U(1)_A$ symmetry: the connected part is dominated by the $U(1)_A$ susceptibility defined as $\sum_x \langle P^a(x) P^a(0) - S^a(x) S^a(0)\rangle$, where $S^a(x)$ and $P^a(x)$ are iso-triplet scalar and pseudoscalar operators, and the disconnected part is governed by the topological susceptibility, which measures the instanton number variance. Meanwhile, the $SU(2)_L \times SU(2)_R$ susceptibilities remain small even when the chiral condensate and $U(1)_A$ susceptibility become nonzero due to finite quark masses.

This result suggests a possibility that the chiral phase transition is actually driven by the $U(1)_A$ breaking as suggested in the early stage of QCD. In Ref. [16], it was argued that if the $U(1)_A$ breaking is kept large at the critical temperature the transition is likely to be the second order. But if the $U(1)_A$ symmetry effectively "emerges", the order or the universality class of the transition differs from the naive expectation, which would require changes in the current understanding of the early universe.

2. Dirac eigenmode decomposition of susceptibilities

Let us start with the N_f-flavor QCD partition function with a nonzero vacuum angle θ,

$$Z(m,\theta) = \int [dA] \det(D(A) + m)^{N_f} e^{-S_G(A) + i\theta Q(A)}, \tag{1}$$

where the path integral over the gauge field A is performed with a weight given by the gauge action $S_G(A)$, topological charge $Q(A)$, or equivalently the index of the Dirac operator $D(A)$, and the fermion determinant with a degenerate quark mass m. We have used a continuum notation for simplicity. The lattice formulas in terms of the overlap-Dirac operator [17] will be given later.

Denoting the eigenvalues of $D(A)$ by $i\lambda(A)$, among which every nonzero mode appears in a pair with its conjugate $-i\lambda(A)$, the chiral condensate at $\theta = 0$ is decomposed as

$$\Sigma(m) = \frac{1}{N_f V} \frac{\partial}{\partial m} \ln Z(m,0) = \frac{1}{V} \left\langle \sum_{\lambda(A)} \frac{m}{\lambda(A)^2 + m^2} \right\rangle. \tag{2}$$

Here and in the following, the expectation value of a quantity $X(A)$ (with $\theta = 0$) is written as $\langle X(A)\rangle$.

The chiral susceptibility, defined as a derivative of $\Sigma(m)$ with respect to m, may be decomposed into two parts. The "connected" susceptibility $\chi^{\text{con.}}(m)$ is a derivative of the chiral condensate with respect to the valence quark mass m_v, while the "disconnected" part $\chi^{\text{dis.}}(m)$ is that with respect to the sea quark mass m_s, setting $m_v = m_s = m$ for both.

In the connected susceptibility, we have a term $\Sigma(m)/m$, which is a unique source of a quadratic divergence, while other pieces are only logarithmically divergent. To remove this quadratic divergence, we introduce a subtracted condensate $\Sigma_{\text{sub.}}(m)$,

$$\frac{\Sigma_{\text{sub.}}(m)}{m} = \left[\frac{\Sigma(m)}{m} - \frac{\langle|Q(A)|\rangle}{m^2 V}\right] - \left[\frac{\Sigma(m_{\text{ref}})}{m_{\text{ref}}} - \frac{\langle|Q(A)|\rangle|_{m=m_{\text{ref}}}}{m_{\text{ref}}^2 V}\right], \tag{3}$$

with a reference quark mass m_{ref}. The term with $|Q(A)|$ eliminates the contribution from chiral zero modes, which is expected to vanish in the large-V limit.

The connected susceptibility (with the subtraction above) can be written as

$$\chi^{\text{con.}}_{\text{sub.}}(m) = -\Delta^{\text{con.}}_{U(1)}(m) + \frac{\Sigma_{\text{sub.}}(m)}{m} + \frac{\langle|Q(A)|\rangle}{m^2 V}, \tag{4}$$

where

$$\Delta^{\text{con.}}_{U(1)}(m) = \frac{1}{V}\left\langle \sum_{\lambda(A)} \frac{2m^2}{(\lambda(A)^2 + m^2)^2} \right\rangle \tag{5}$$

is equivalent to the axial $U(1)$ susceptibility $\sum_x[\langle P^a(x)P^a(0)\rangle - \langle S^a(x)S^a(0)\rangle]$ (see Refs. [13,14] for details). On the other hand, the eigenvalue decomposition of the disconnected part is

$$\chi^{\text{dis.}}(m) = \frac{N_f}{V}\left[\left\langle\left(\sum_{\lambda(A)} \frac{m}{\lambda(A)^2 + m^2}\right)^2\right\rangle - (\Sigma(m)V)^2\right]. \tag{6}$$

From the θ dependence of $Z(m,\theta)$, we obtain the topological susceptibility:

$$\chi_t(m) = -\frac{1}{V}\frac{\partial^2}{\partial\theta^2}\ln Z(m,\theta)\,|_{\theta=0} = \frac{\langle Q(A)^2\rangle - \langle Q(A)\rangle^2}{V}. \tag{7}$$

Absorbing the angle θ into the mass term $m \to m\exp(i\gamma_5\theta/N_f)$, we can relate $\chi_t(m)$ to the chiral condensate and the pseudoscalar susceptibility $\sum_x\langle P^0(x)P^0(0)\rangle$:

$$\chi_t(m) = m\left[\frac{\partial}{\partial\theta}\langle\bar{q}i\gamma_5 e^{i\gamma_5\theta/N_f}q\rangle_\theta\right]\Big|_{\theta=0} = -\sum_x\langle P^0(x)P^0(0)\rangle - \frac{\Sigma(m)}{m}. \tag{8}$$

We can now see that the $U(1)_A$ and $SU(2)_L \times SU(2)_R$ symmetries are intimately related [18,19]. Two possible probes of the $SU(2)_L \times SU(2)_R$ symmetry given by

$$\Delta^{(1)}_{SU(2)}(m) \equiv \sum_x\langle S^0(x)S^0(0) - P^a(x)P^a(0)\rangle - V\langle S^0(0)\rangle^2 = \chi^{\text{dis.}}(m) - \Delta^{\text{con.}}_{U(1)}(m), \tag{9}$$

$$\Delta^{(2)}_{SU(2)}(m) \equiv \sum_x\langle S^a(x)S^a(0) - P^0(x)P^0(0)\rangle = \frac{N_f}{m^2}\chi_t(m) - \Delta^{\text{con.}}_{U(1)}(m) \tag{10}$$

are actually written using the $U(1)_A$ related quantities $\Delta^{\text{con.}}_{U(1)}(m)$, $\chi_t(m)$, and $\chi^{\text{dis.}}(m)$. When the axial $U(1)$ anomaly is active so that $\Delta^{\text{con.}}_{U(1)}(m)$ [20–26] is nonzero, the recovery of the $SU(2)_L \times SU(2)_R$ requires fine tuning:

$$\lim_{m\to 0}\chi^{\text{dis.}}(m) = \lim_{m\to 0}\Delta^{\text{con.}}_{U(1)}(m) = \lim_{m\to 0}\frac{N_f}{m^2}\chi_t(m), \tag{11}$$

which is highly nontrivial.

From Eqs. (4), (9), and (10), we can separate the $U(1)_A$ breaking contributions $\chi_A^{\text{con.}}(m)$ and $\chi_A^{\text{dis.}}(m)$ from the connected and disconnected parts of the chiral susceptibility, $\chi_{\text{sub.}}^{\text{con.}}(m)$ and $\chi^{\text{dis.}}(m)$ respectively, as

$$\chi_A^{\text{con.}}(m) = -\Delta_{U(1)}^{\text{con.}}(m) + \frac{\langle |Q(A)| \rangle}{m^2 V}, \tag{12}$$

$$\chi_A^{\text{dis.}}(m) = \frac{N_f}{m^2}\chi_t(m). \tag{13}$$

Then the remnants are $\chi_{\text{sub.}}^{\text{con.}}(m) - \chi_A^{\text{con.}}(m) = \Sigma_{\text{sub.}}(m)/m$ and $\chi^{\text{dis.}}(m) - \chi_A^{\text{dis.}}(m) = \Delta_{SU(2)}^{(1)}(m) - \Delta_{SU(2)}^{(2)}(m)$, respectively.

These formulas can be promoted to those of lattice QCD with the overlap fermion [13]. Denoting the eigenvalue of the massive overlap-Dirac operator $\gamma_5((1-m)D_{\text{ov}} + m)$ by λ_m, the eigenvalue decomposition can be obtained by replacing $\frac{1}{\lambda(A)^2+m^2}$ with $\frac{(1-\lambda_m^2)}{(1-m^2)\lambda_m^2}$ (here and in the following, we take the lattice spacing as unity). In the following we numerically study how much the $U(1)_A$-related pieces $\chi_A^{\text{con./dis.}}(m)$ dominate the signal of the chiral susceptibility in $N_f = 2$ lattice QCD. We employ a lattice fermion formulation that precisely preserves chiral symmetry, which is essential in the above formulas with spectral decomposition.

3. Lattice simulation

We use the gauge field ensembles generated in Ref. [15]. We employ the tree-level improved Symanzik gauge action and the Möbius domain-wall fermion [27,28] action for the simulations. We include the overlap fermion determinant utilizing a reweighting technique in order to eliminate systematics due to any violation of the chiral symmetry, as well as those due to the mixed action. The lattice spacing is fixed to $a = 0.074$ fm, and four different temperatures are chosen taking a set of the temporal lattice extent $L_t = 8, 10, 12$, and 14, which covers $190 \leq T \leq 330$ MeV. We fix the lattice size to $L = 32$, which corresponds to 2.4 fm. At $T = 220$ MeV, three different lattice sizes $L = 24, 32, 40$ are taken in order to check if the finite volume effect is under control. The range of quark mass covers the physical up and down quark mass, estimated to be $m = 0.0014(2)$ from the pion mass $m_\pi = 0.135(8)$ at $T = 0$ and $m = 0.01$. We use $m = 0.005$, which is the highest quark mass at $T = 190$ MeV simulations, on $L = 32$ lattices as the reference point m_{ref} for the subtraction of the connected chiral susceptibility.

We compute the 40 lowest eigenvalues of the massive overlap-Dirac operator, as well as those of the 4D effective operator of the Möbius domain-wall fermion. For both operators, we can identify the index $Q(A)$ as the number of isolated chiral zero modes. At the lowest temperature, the 40th eigenvalue is $\sim$0.08 ($\sim$210 MeV).

Since the number of stored eigenvalues is limited, we truncate the summation in the spectral decomposition of the chiral susceptibilities. In Fig. 1, we plot the cut-off dependence of the (subtracted) chiral susceptibilities. We find for $T \leq 260$ MeV, both $\chi_{\text{sub.}}^{\text{con.}}$ and $\chi^{\text{dis.}}$ with the reweighted overlap fermion show a good saturation already at $\lambda = 0.07$ in all the simulated ensembles. At $T = 260$ MeV, we also find a good agreement with a full measurement without the truncation computed with the Möbius domain-wall Dirac operator. At $T = 330$ MeV, on the other hand, the low-mode approximation does not reproduce the full result, especially at heavier quark masses. In our previous study [15] we found that at this temperature the low-lying modes are almost absent and the observables are insensitive to the violation of the lattice chiral symmetry. Therefore, in the following analysis at $T = 330$ MeV, we take the full computation with the Möbius domain-wall Dirac operator and use the low-mode

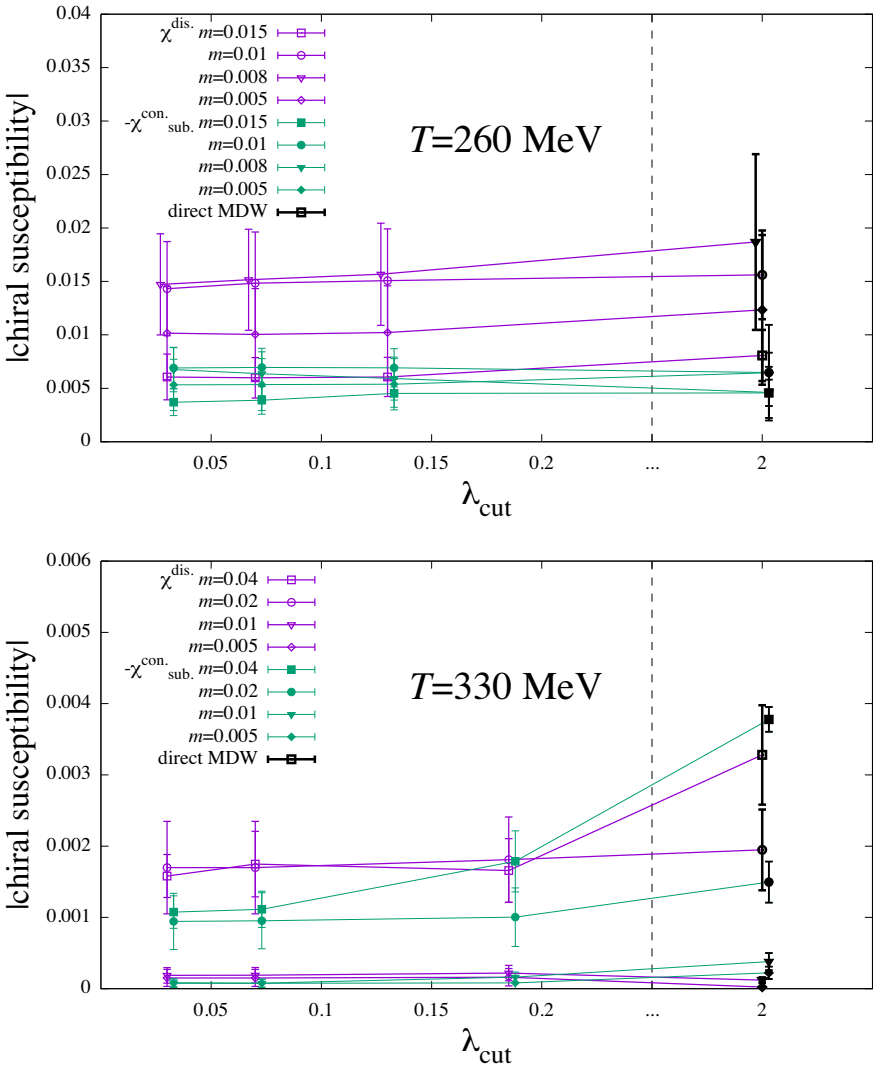

Fig. 1. Cut-off $\lambda_{\rm cut}$ dependence of the chiral susceptibility at $T = 260$ MeV (top) and $T = 330$ MeV (bottom). The result for $\chi^{\rm dis.}$ is plotted by open symbols, while that for $-\chi^{\rm con.}_{\rm sub.}$ is shown by filled symbols. The thick symbols plotted at the lattice cut-off =2 denote those obtained from the direct inversion of the Möbius domain-wall operator.

approximation of the overlap-Dirac fermion at $\lambda_{\rm cut} = 0.07$ (∼180 MeV) for other ensembles of $T \leq 260$ MeV.

The statistical uncertainty is estimated by the jackknife method after binning the data in every 1000 trajectories with which the autocorrelation is negligible.

4. Numerical results

We summarize our numerical results in Table 1.

In Fig. 2, we present the results for the connected part $\chi^{\rm con.}_{\rm sub.}$ (top) and disconnected data $\chi^{\rm dis.}$ (bottom) of the chiral susceptibility at $T = 220$ MeV on the $L = 32$ lattice (open squares). The filled symbols are those of $\chi^{\rm con.}_A$ and $\chi^{\rm dis.}_A$, which dominate the signals. The other contributions $\Sigma_{\rm sub.}(m)/m$ (circles) and the $SU(2)$ susceptibilities $\Delta^{(1,2)}_{SU(2)}(m)$ (circles and triangles) are relatively small. This result indicates that the connected part of the subtracted chiral susceptibility is essentially described by the axial $U(1)$ susceptibility and the disconnected susceptibility

Table 1. Summary of results.

T (MeV)	$L^3 \times L_t$	m	$\chi^{\text{con.}}_{\text{sub.}}$	$\chi^{\text{con.}}_A$	$\chi^{\text{dis.}}$	$\chi^{\text{dis.}}_A$
190	$32^3 \times 14$	0.005	−0.074(07)	−0.074(12)	0.090(12)	0.077(17)
		0.003 75	−0.101(20)	−0.106(26)	0.144(39)	0.189(49)
		0.0025	−0.058(12)	−0.056(11)	0.087(15)	0.079(21)
		0.001	−0.0188(64)	−0.001 30(45)	0.0020(06)	$1.6(16) \times 10^{-7}$
220	$24^3 \times 12$	0.01	−0.0224(23)	−0.0202(34)	0.0399(75)	0.0338(68)
		0.005	−0.0367(87)	−0.0332(88)	0.066(20)	0.072(24)
		0.003 75	−0.0081(28)	−0.0041(27)	0.0079(52)	0.0070(53)
		0.0025	−0.0125(55)	−0.0095(54)	0.019(11)	0.018(11)
		0.001	−0.0033(25)	−0.0002(01)	0.000 33(24)	0(0)
	$32^3 \times 12$	0.01	−0.0284(25)	−0.0325(38)	0.044(07)	0.049(11)
		0.005	−0.0311(42)	−0.0311(48)	0.065(11)	0.068(14)
		0.003 75	−0.006 82(83)	−0.002 70(70)	0.0050(13)	0.003 8(13)
		0.0025	−0.0073(49)	−0.0062(48)	0.0121(94)	0.0112(95)
		0.001	−0.0016(12)	−0.000 16(06)	0.000 30(12)	$1.8(18) \times 10^{-5}$
	$40^3 \times 12$	0.01	−0.0270(15)	−0.0349(28)	0.0417(56)	0.0397(49)
		0.005	−0.0305(31)	−0.0371(56)	0.0526(65)	0.0433(54)
260	$32^3 \times 10$	0.015	−0.0039(13)	−0.0038(14)	0.0060(19)	0.0061(24)
		0.01	−0.0070(18)	−0.0077(24)	0.0148(48)	0.0141(43)
		0.008	−0.0064(20)	−0.0089(32)	0.0152(47)	0.0117(38)
		0.005	−0.0054(24)	−0.0054(24)	0.0100(43)	0.0103(45)
330	$32^3 \times 8$	0.040	−0.003 78(17)	−0.003 06(21)	0.003 28(70)	0.002 19(40)
		0.020	−0.001 50(29)	−0.001 45(30)	0.001 95(57)	0.001 48(49)
		0.015	−0.001 45(65)	−0.001 51(82)	0.0027(19)	0.0017(11)
		0.01	−0.000 386(95)	−0.000 183(62)	0.000 12(03)	0.000 44(31)
		0.005	−0.000 222(87)	−0.000 222(77)	$2.33(53) \times 10^{-5}$	0(0)
		0.001	−0.000 10(10)	$-2.81(58) \times 10^{-5}$	$8.6(14) \times 10^{-7}$	0(0)

is governed by the topological susceptibility[1]. The axial $U(1)$ breaking contributions $\chi^{\text{con.}}_A$ and $\chi^{\text{dis.}}_A$ are strongly suppressed at the lightest quark mass. In the data with different lattice sizes $L = 24$ (crosses) and 40 (stars), no significant volume dependence is seen. The data may indicate a peak at $m = 0.005$.

These features are seen at all simulated temperatures and quark masses ranging from the physical point to $m \sim 100$ MeV. Figure 3 summarizes the quark mass dependence of the connected (top) and disconnected (bottom) chiral susceptibility at four different temperatures on the $L = 32$ lattices. The open symbols with solid lines are the data obtained from the eigenmode decomposition of the reweighted overlap-Dirac operator, while those with dotted lines are from direct measurement with the Möbius domain-wall fermion. At each temperature, the axial $U(1)$ breaking effect $\chi^{\text{con./dis.}}_A$ (filled symbols with dashed lines) dominates the signal of the susceptibility. It is remarkable that this dominance is seen even at higher quark mass regions than the peaks, where both $SU(2)_L \times SU(2)_R$ and $U(1)_A$ are expected to be sizably broken. In fact, we find that simple sums of $\chi^{\text{con.}}_A$ and $\chi^{\text{dis.}}_A$ over 26 simulated data points are $-0.48(2)$ and $0.74(6)$, respectively, while those of $\chi^{\text{con.}}_{\text{sub.}}$ and $\chi^{\text{dis.}}$ are $-0.50(2)$ and $0.73(4)$. They differ by only 3% and 1% and within standard deviation. Also, we note that the axial $U(1)$ breaking contributions are strongly suppressed near the chiral limit.

We also plot the result obtained in our previous work with $\beta = 4.24$ on a coarser lattice ($a = 0.084$ fm) at $T = 195$ MeV (cross symbols). The result is consistent with our new data at a similar temperature $T = 190$ MeV, which indicates that the cut-off effect is not significant.

[1] It was pointed out in Refs. [22,25] that $\chi^{\text{dis.}}$ is dominated by $U(1)_A$ breaking in the $m = 0$ limit, but the concrete form (in terms of the topological susceptibility) at finite m was not discussed.

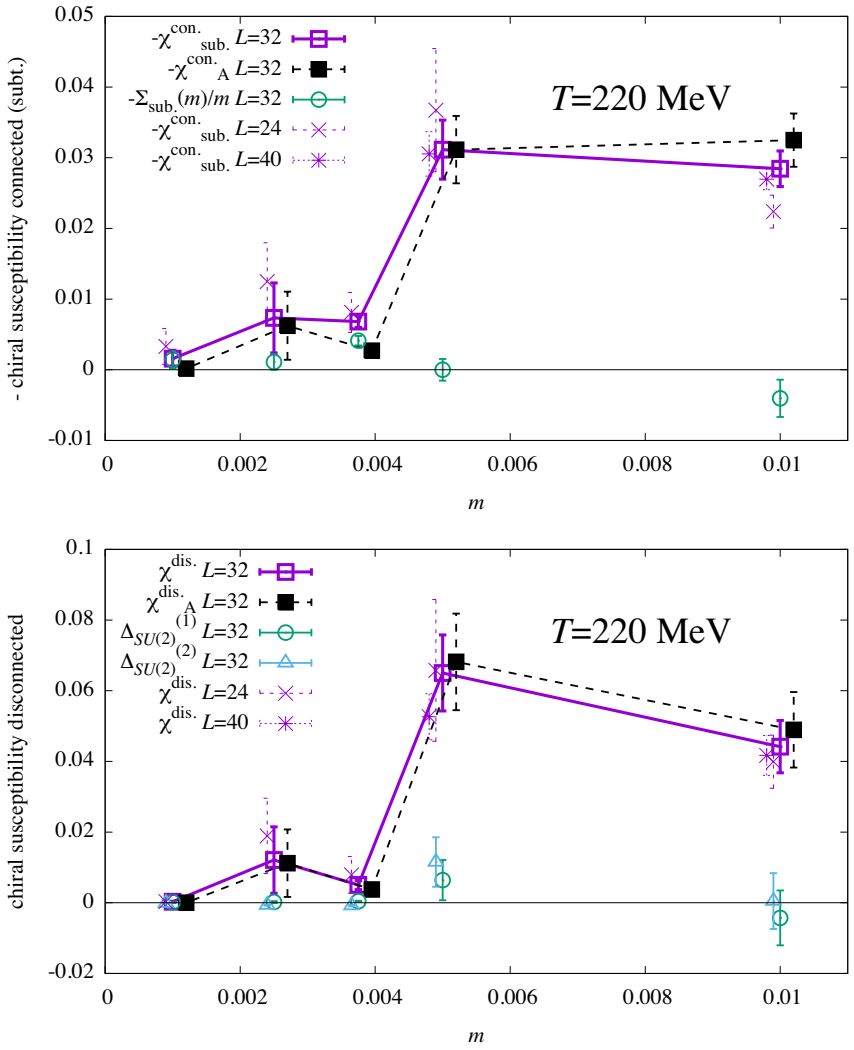

Fig. 2. Quark mass dependence of the connected (top) and disconnected (bottom) chiral susceptibilities on the $L = 32$ lattice (open squares). The contribution from the axial $U(1)$ breaking (filled squares) saturates the signal, while the remaining $\Sigma_{\text{sub.}}(m)/m$ and $\Delta^{(1,2)}_{SU(2)}(m)$ plotted by open circles and triangles are small. The $L = 24$ (crosses) and $L = 40$ (stars) data show no significant volume dependence. Note that the sign of the connected part is flipped.

In Fig. 3 the position of the peak moves towards heavier quark masses as temperature increases. This indicates that our simulated temperatures cover the pseudocritical temperature, which becomes higher for larger quark masses[2].

In the total contribution $\chi^{\text{con.}}_{\text{sub.}}(m) + \chi^{\text{dis.}}(m)$, however, the situation is not so simple. As shown in Fig. 4, the $U(1)_A$ breaking dominance by

$$\chi^{\text{con.}}_A(m) + \chi^{\text{dis.}}_A(m) = -\Delta^{\text{con.}}_{U(1)}(m) + \frac{N_f}{m^2}\chi_t(m) + \frac{\langle|Q(A)|\rangle}{m^2 V} \tag{14}$$

is still visible. But the smallness of $\Delta^{(1),(2)}_{SU(2)}(m)$ implies $\Delta^{\text{con.}}_{U(1)}(m) \sim \frac{N_f}{m^2}\chi_t(m)$ so that the quantity is dominated by the last term $\frac{\langle|Q(A)|\rangle}{m^2 V}$, which is expected to vanish in the thermodynamical limit. Therefore, in order to quantify the axial $U(1)$ breaking effect in the total contribution, we need

[2]A strong increase of the pseudocritical temperature has been reported in 2+1-flavor lattice QCD simulations [9].

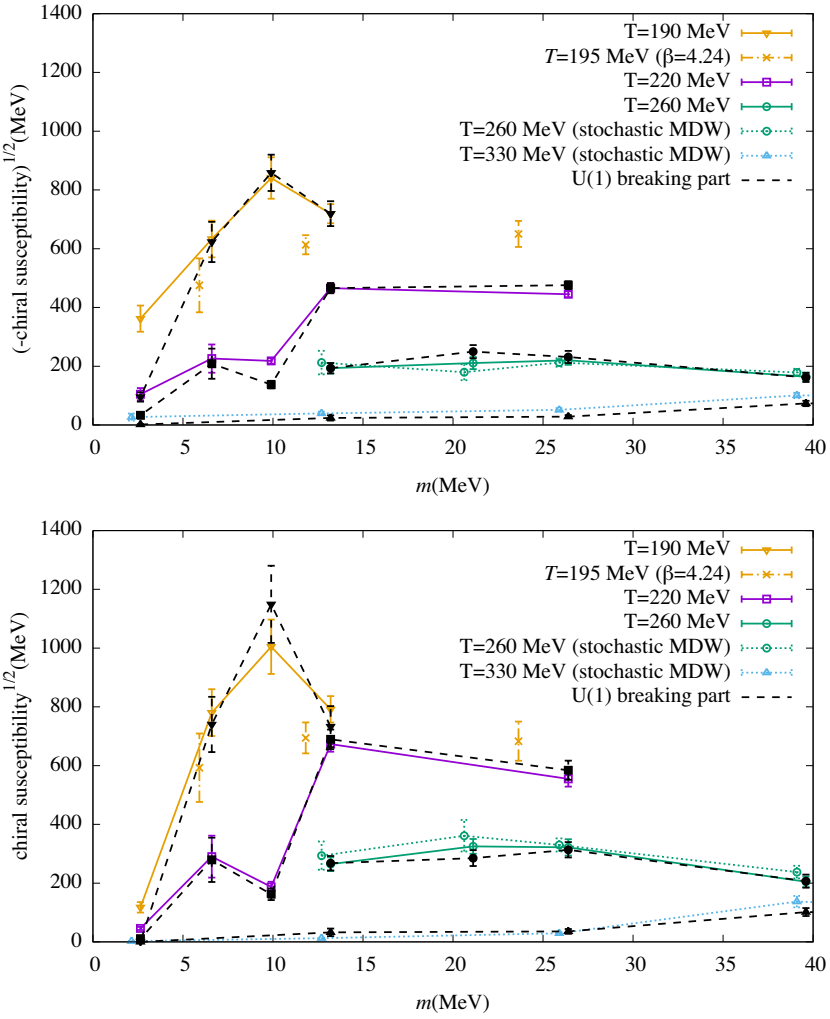

Fig. 3. Chiral susceptibility at four different temperatures on the $L = 32$ lattices (open symbols).The connected (top) and disconnected (bottom) parts are shown. The filled symbols are those from axial $U(1)$ breaking.

a careful analysis of the delicate cancellation between $\Delta^{\text{con.}}_{U(1)}(m)$ and $\frac{N_f}{m^2}\chi_t(m)$, as well as their large-volume limits. Although such a fine analysis is beyond the scope of this work, let us try to raise two possible scenarios. The first one is that the signal of the total susceptibility gets smaller as the volume increases and is eventually given by the tiny quark mass dependence of the $SU(2)_L \times SU(2)_R$ breaking. The second is that even when $\frac{\langle|Q(A)|\rangle}{m^2V}$ disappears in the large-volume limit, the near-chiral-zero modes in $\Sigma_{\text{sub.}}(m)$ compensate its absence and keep the total susceptibility insensitive to the volume. In Fig. 5, we plot $\frac{\Sigma_{\text{sub.}}(m)}{m} + \frac{\langle|Q(A)|\rangle}{m^2V}$ (open and solid symbols) and $\frac{\langle|Q(A)|\rangle}{m^2V}$ (filled and dashed) as functions of the lattice size L. The consistency of the former at $L = 32$ and 40 in spite of the decrease of the latter may be support for the second scenario.

We conclude that the connected and disconnected chiral susceptibilities are dominated by the axial $U(1)$ breaking effects at temperatures $T \gtrsim 190$ MeV, which covers the pseudocritical temperature when the quark mass is finite. The connected part is described by the axial $U(1)$ susceptibility other than the m-independent quadratically divergent part, and the disconnected part is governed by the topological susceptibility. The chiral limit of the $U(1)_A$ contributions is

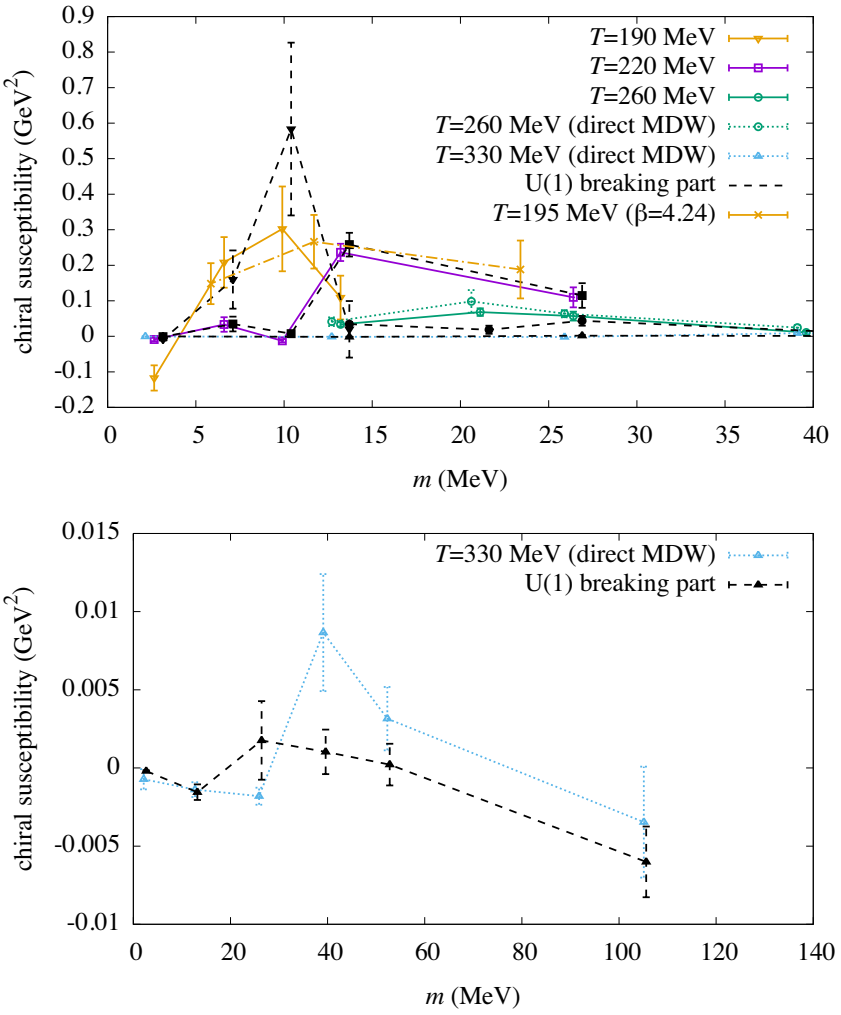

Fig. 4. Chiral susceptibility at four different temperatures on the $L = 32$ lattices (open symbols). The filled symbols are those from axial $U(1)$ breaking. The bottom panel is the same as the top but the result at $T = 330$ MeV is shown on a fine scale.

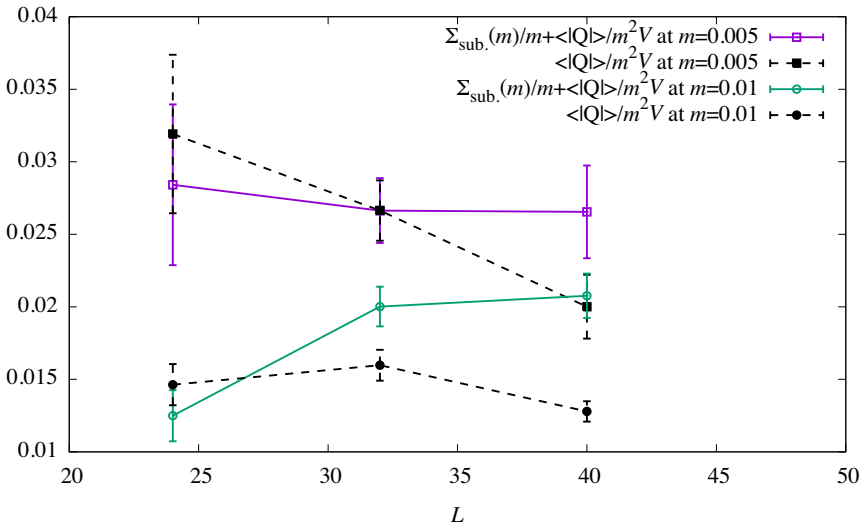

Fig. 5. The lattice size L dependence of $\frac{\Sigma_{\text{sub.}}(m)}{m} + \frac{\langle |Q(A)| \rangle}{m^2 V}$ (open symbols connected by solid lines) and $\frac{\langle |Q(A)| \rangle}{m^2 V}$ (filled symbols connected by dashed lines). The data at $m = 0.01$ and 0.005 are presented.

strongly suppressed. The picture of the QCD phase diagram [16], based on spontaneous $SU(2)_L \times SU(2)_R$ breaking alone, may need to be reconsidered, or a delicate cancellation between the connected and disconnected parts of the $U(1)_A$ breaking is, at least, required. It turns out that axial $U(1)$ breaking does play a crucial role.

Acknowledgments

We thank H.-T. Ding, C. Gattringer, and L. Glozman for useful discussions. We thank P. Boyle for correspondence on the Grid starting simulation and I. Kanamori for helping us with the simulations on the K computer with Bridge++. We also thank the members of the JLQCD Collaboration for their encouragement and support. We thank the Yukawa Institute for Theoretical Physics at Kyoto University. Discussions during the YITP workshop YITP-W-20-08 on "Progress in Particle Physics 2020" were useful in completing this work. Numerical simulations were performed using the QCD software packages Iroiro++ [29], Grid [30], and Bridge++ [31] on the IBM System Blue Gene Solution at KEK with the support of its Large Scale Simulation Program (No. 16/17-14) and Oakforest-PACS at JCAHPC with the support of the HPCI System Research Projects (Project IDs: hp170061, hp180061, hp190090, and hp200086), the Multidisciplinary Cooperative Research Program in CCS, University of Tsukuba (Project IDs: xg17i032 and xg18i023), and the K computer provided by the RIKEN Center for Computational Science. We used the Japan Lattice Data Grid (JLDG) [32] for storing some of the numerical data generated for this work. This work is supported in part by Japanese Grants-in-Aid for Scientific Research (Nos. JP26247043, JP16H03978, JP18H01216, JP18H03710, JP18H04484, JP18H05236), by MEXT as a "Priority Issue on Post-K Computer" (Elucidation of the Fundamental Laws and Evolution of the Universe), and by the Joint Institute for Computational Fundamental Science (JICFuS).

Funding

Open Access funding: SCOAP[3].

Appendix. Comparison with Ding et al. [25]

Recently, Ding et al. [25] investigated the disconnected part of chiral susceptibility in $N_f = 2 + 1$ QCD using eigenvalues of the Dirac operator of highly improved staggered quark (HISQ) action. At $T = 207$ MeV they obtained a nonzero continuum limit, which suggests that the axial $U(1)$ symmetry is still broken by an anomaly at 1.6 T_c. As their conclusion qualitatively differs from ours, which becomes consistent with zero at the lightest simulated quark mass, here we would like to compare the two.

In Fig. A1 we represent the data from Ref. [25] by open symbols and those of this work by filled symbols. Since the strange quark is quenched in our simulations, we simply use the physical value of the strange quark mass for m_s. Note that the critical temperature is estimated to be $\sim$130 MeV for $N_f = 2 + 1$, QCD while it is $\sim$170 MeV for $N_f = 2$. Interestingly, the qualitative feature of sharp drops towards the chiral limit is similar. However, a significant cutoff $1/a$ dependence is seen in Ref. [25]; the data at $a = 0.06$ fm are twice as large as those at $a = 0.08$ fm, while our data at $a = 0.08$ fm ($T = 195$ MeV) and $a = 0.07$ fm ($T = 190$ MeV) do not show such a sizable discretization effect.

In Ref. [25] they obtained a continuum limit with a global fit with six parameters, which is shown by the dashed curve in Fig. A1. It is clearly higher than the raw data at finite lattice spacings. Specifically, the one at the second lightest quark mass at $a = 0.12$ fm is extrapolated to a continuum limit that is 40 times larger, which suggests that their lattice data are not on a proper scaling trajectory that allows continuum extrapolation assuming an expansion in a^2. Since the $U(1)_A$ anomaly does not correctly couple to the taste singlet component of the stag-

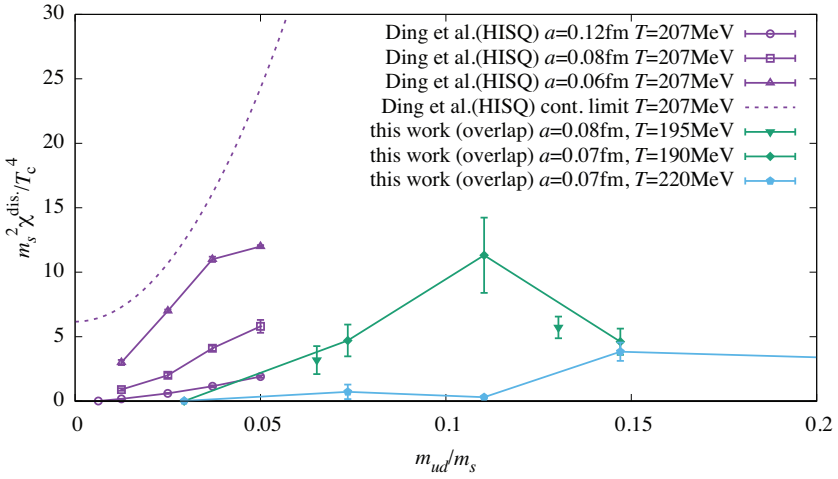

Fig. A1. Comparison of $\chi^{\rm dis.}(m)$ between Ding et al. [25] (open symbols) and this work (filled). The qualitative feature of a sharp drop towards the chiral limit is similar. But the large scaling violation in Ref. [25] leads to a continuum limit much larger than the raw values, as shown by the dashed curve.

gered fermion that Ref. [25] employed, the quantities that are strongly affected by the chiral anomaly and index theorem may be subject to large discretization effects in their simulation.

References

[1] F. Karsch and E. Laermann, Phys. Rev. D **50**, 6954 (1994) [arXiv:hep-lat/9406008 [hep-lat]] [Search INSPIRE].
[2] Y. Aoki, G. Endrodi, Z. Fodor, S. D. Katz, and K. K. Szabo, Nature **443**, 675 (2006) [arXiv:hep-lat/0611014 [hep-lat]] [Search INSPIRE].
[3] M. Cheng et al., Phys. Rev. D **74**, 054507 (2006) [arXiv:hep-lat/0608013 [hep-lat]] [Search INSPIRE].
[4] A. Bazavov et al. [HotQCD Collaboration], Phys. Rev. D **85**, 054503 (2012) [arXiv:1111.1710 [hep-lat]] [Search INSPIRE].
[5] T. Bhattacharya et al. [HotQCD Collaboration], Phys. Rev. Lett. **113**, 082001 (2014) [arXiv:1402.5175 [hep-lat]] [Search INSPIRE].
[6] C. Bonati, M. D'Elia, M. Mariti, M. Mesiti, F. Negro, and F. Sanfilippo, Phys. Rev. D **92**, 054503 (2015).
[7] B. B. Brandt, A. Francis, H. B. Meyer, O. Philipsen, D. Robaina, and H. Wittig, J. High Energy Phys. **1612**, 158 (2016) [arXiv:1608.06882 [hep-lat]] [Search INSPIRE].
[8] Y. Taniguchi et al. [WHOT-QCD Collaboration], Phys. Rev. D **96**, 014509 (2017) Erratum: Phys.Rev.D 99 (2019) 5, 059904 [arXiv:1609.01417 [hep-lat]] [Search INSPIRE].
[9] H. T. Ding et al. [HotQCD Collaboration], Phys. Rev. Lett. **123**, 062002 (2019) [arXiv:1903.04801 [hep-lat]] [Search INSPIRE].
[10] C. G. Callan Jr, R. F. Dashen, and D. J. Gross, Phys. Rev. D **17**, 2717 (1978).
[11] D. Diakonov and V. Y. Petrov, Phys. Lett. B **147**, 351 (1984).
[12] S. Aoki, H. Fukaya, and Y. Taniguchi, Phys. Rev. D **86**, 114512 (2012) [arXiv:1209.2061 [hep-lat]] [Search INSPIRE].
[13] G. Cossu et al. [JLQCD Collaboration], Phys. Rev. D **93**, 034507 (2016) [arXiv:1510.07395 [hep-lat]] [Search INSPIRE].
[14] A. Tomiya et al. [JLQCD Collaboration], Phys. Rev. D 96, 034509 (2017) **96**, 079902 (2017) [addendum] [arXiv:1612.01908 [hep-lat]] [Search INSPIRE].
[15] S. Akoi et al. [JLQCD Collaboration], Phys. Rev. D **103**, 074506 [arXiv:2011.01499] [Search INSPIRE].
[16] R. D. Pisarski and F. Wilczek, Phys. Rev. D **29**, 338 (1984).
[17] H. Neuberger, Phys. Lett. B **417**, 141 (1998) [arXiv:hep-lat/9707022] [Search INSPIRE].

[18] A. Gómez Nicola and J. Ruiz De Elvira, Phys. Rev. D **98**, 014020 (2018) [arXiv:1803.08517 [hep-ph]] [Search INSPIRE].
[19] A. G. Nicola, Eur. Phys. J. Spec. Top. **230**, 1645 (2021) [arXiv:2012.13809 [hep-ph]] [Search INSPIRE].
[20] A. Bazavov et al. [HotQCD Collaboration], Phys. Rev. D **86**, 094503 (2012) [arXiv:1205.3535 [hep-lat]] [Search INSPIRE].
[21] G. Cossu, S. Aoki, H. Fukaya, S. Hashimoto, T. Kaneko, H. Matsufuru, and J.-I. Noaki, Phys. Rev. D **87**, 114514 (2013) Erratum: Phys.Rev.D 88 (2013) 1, 019901[arXiv:1304.6145] [Search INSPIRE].
[22] M. I. Buchoff et al. [LLNL/RBC Collaboration], Phys. Rev. D **89**, 054514 (2014) [arXiv:1309.4149 [hep-lat]] [Search INSPIRE].
[23] V. Dick, F. Karsch, E. Laermann, S. Mukherjee, and S. Sharma, Phys. Rev. D **91**, 094504 (2015) [arXiv:1502.06190 [hep-lat]] [Search INSPIRE].
[24] K.-I. Ishikawa, Y. Iwasaki, Y. Nakayama, and T. Yoshie; arXiv:1706.08872 [hep-lat] [Search INSPIRE].
[25] H. T. Ding, S. T. Li, S. Mukherjee, A. Tomiya, X. D. Wang, and Y. Zhang, Phys. Rev. Lett. **126**, 082001 (2021) [arXiv:2010.14836 [hep-lat]][Search INSPIRE].
[26] O. Kaczmarek, L. Mazur, and S. Sharma, arXiv:2102.06136 [hep-lat] [Search INSPIRE].
[27] R. C. Brower, H. Neff, and K. Orginos, Nucl. Phys. Proc. Suppl. **153**, 191 (2006) [arXiv:hep-lat/0511031] [Search INSPIRE].
[28] R. C. Brower, H. Neff, and K. Orginos, Comput. Phys. Commun. **220**, 1 (2017) [arXiv:1206.5214 [hep-lat]] [Search INSPIRE].
[29] G. Cossu, J. Noaki, S. Hashimoto, T. Kaneko, H. Fukaya, P. A. Boyle, and J. Doi, Proceedings of Science **187** 482 [arXiv:1311.0084] [Search INSPIRE].
[30] P. Boyle, A. Yamaguchi, G. Cossu, and A. Portelli, arXiv:1512.03487 [hep-lat] [Search INSPIRE].
[31] S. Ueda, S. Aoki, T. Aoyama, K. Kanaya, H. Matsufuru, S. Motoki, Y. Namekawa, H. Nemura, Y. Taniguchi, and N. Ukita, J. Phys. Conf. Ser. **523**, 012046 (2014).
[32] T. Amagasa et al., J. Phys. Conf. Ser. **664**, 042058 (2015).